ACS APPLIED MATERIALS & INTERFACES

Research Article

www.acsami.org

General Scalable Strategy toward Heterogeneously Doped Hierarchical Porous Graphitic Carbon Bubbles for Lithium-Ion Battery Anodes

Huawei Song, Gongzheng Yang, and Chengxin Wang*

State Key Laboratory of Optoelectronic Materials and Technologies, School of Physics Science and Engineering, Sun Yat-sen (Zhongshan) University, Guangzhou 510275, People's Republic of China

ABSTRACT: Novel carbon nanostructures, e.g., carbon nanotubes (CNTs), graphene, hierarchical porous graphitic carbon (HPGC), and ordered mesoporous carbon (CMK-3), have been significantly forwarding the progress of energy storage and conversion. Advanced electrodes or hybrid electrodes based on them are springing up one after another. To step further, a generic synthetic approach to large scale hierarchical porous graphitic carbon microbubbles (HPGCMBs) is developed by zinc powder templated organic precursor impregnation method. The facile technique features scalable (yield: once more than 200 mg), in situ heteroatom's doping (doping ratio: more than 26%) and hierarchical-pore-creating traits (pore volume: 1.01 $cm^3\ g^{-1}$). Adjustable graphitic content, doping species and amount are readily realized through varying the organic precursors. Rationally, good conductivity, fast kinetics, and abundant ion reservoirs are entirely achieved. To be applied in practice, state-of-the-art anodes for lithium-ion batteries are fabricated. Benefiting from the large specific surface area, rich heteroatoms, and hierarchical pores, the HPGCMBs electrodes exhibit excellent electrochemical properties. Besides superior storage capability of more than 1000 mAh g^{-1} at 100 mA g^{-1}, stable cycling and excellent retention of 370 mAh g^{-1} at large rate of 10 A g^{-1} are achieved in the meantime.

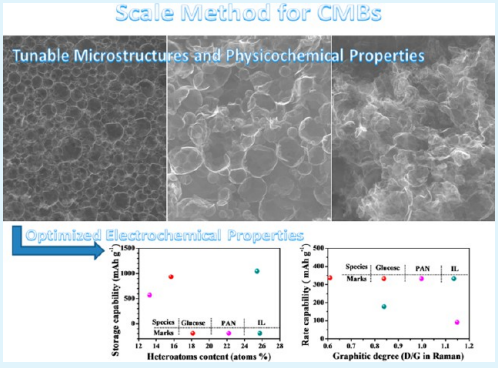

KEYWORDS: *scalable strategy, heteroatom-doped, hierarchical pores, graphitic carbon microbubbles, Lithium ion battery*

INTRODUCTION

With the emerging of energy-intensive portable electronics, electric vehicles, and smart grids, it is urgently demanding to fabricate advanced powering devices.[1−3] Lithium ion batteries (LIBs), one of the promising power sources, exhibit high operation voltage, long cycle life, little self-discharge and memory effect, yet are severely compromised in energy and power performance for limited ion storage capability and to-be-improved kinetic processes.[4,5] To address these issues, various high capacity electrode materials (e.g., silicon, germanium, and tin) are explored in novel nanostructures or hybrid composites exhibiting impressive ion storage capability and excellent cyclibility.[6−12] Besides, traditional electrode materials based on graphite are also revisited in novel carbon nanostructures, e.g. carbon nanotubes (CNTs), graphene, hierarchical porous graphitic carbon (HPGC), and ordered mesoporous carbon (CMK-3).[13−23] These nanostructures and composites not only feature small size and large specific surface full of active sites and abundant defects for charge storage but also facilitate ion transport and charge transfer benefiting from their conductive hierarchical porous configurations.

Heterogeneous doping is widely applied in sensing, semiconductor electronics, energy conversion, etc.[16,24−29] Among the various applications, the main roles that the doped atoms have played should at least have something to do with the following aspects: energy-band engineering, defects regulating, and structure stabilizing.[30] Specifically, boron, nitrogen, oxygen, sulfur, fluorine, and phosphorus doped or treated carbon and their composites are extensively focused in energy storage and conversion.[31−35] On the one hand, these heterogeneous atoms enhance the ion storage capability of the host by chemical bonding or physical adsorption.[33,34] On the other hand, the heterogeneous groups themselves may be transformed into more radicals for ion storage.[18,34] Moreover, the disparity in electronic structure endows the heteroatoms with barrier regulating effect.[33,34]

On the basis of the mentioned virtues, the search of universal, scalable, easily available methods to heterogeneously doped novel carbon nanostructures is a meaningful field. Herein, on the basis of our previous work,[36,37] we develop a scalable approach for heterogeneously doped hierarchical porous graphitic carbon microbubbles (HPGCMBs) by organic precursor impregnation zinc powder templated method. To explicate the potential superiority of the strategy, we fabricated various organic precursors derived HPGCMBs and their electrodes for LIBs. Through altering the precursor, the electrochemical properties for the HPGCMBs electrodes are

Received: October 1, 2014
Accepted: November 19, 2014
Published: November 19, 2014

optimized on the basis of the adjustable graphitic content, doping species, and amount.

EXPERIMENTAL DETAILS

1. Material Synthesis. All the reagents were used without purification. HPGCMBs were prepared by an organic precursor impregnation zinc powder templated method followed by a zinc evacuation annealing process. For example, to synthesize the Oxygen-doped HPGCMBs, 5 g zinc powder (Guangdong Guanghua Sci-Tech Co., Ltd., AR) was first impregnated by 0.005 M glucose ethylene glycol solvent ((Guangdong Guanghua Sci-Tech Co., Ltd., AR)), and then the impregnated slurry was held at 300 °C for 1 h to promote the carbonization of glucose; after that, the Zn@carbonized-glucose was annealed at 1000 °C for 1 h to evacuate the zinc template. The whole process was consecutively performed in a tubular furnace under vacuum circumstances. Approximately, 200 mg of HPGCMBs can be attained once. To fabricate other heteroatom-doped HPGCMBs, we could choose various organics containing those heteroatoms as the precursor. Specifically, Nitrogen containing ionic liquid (e.g., 1-alkyl-3-methylimidazolium bromide (Chinese Academy of Science, 99%)), or polyacrylonitrile (PAN) (Sigma-Aldrich, average M_w 150 000, 97%) could be used as the precursors to synthesize nitrogen-doped HPGCMBs; and the nitrogen-, oxygen-, and boron-*co*-doped HPGCMBs can be derived from a nitrogen-and boron-containing ionic liquid (e.g. 1-dodecyl-3- methylimidazolium tetrafluoroborate (Chinese Academy of Science, 99%)). The general synthetic process is also illustrated in Scheme 1 in detail.

Scheme 1. Schematic Illustration for the Synthesis of HPGCMBs

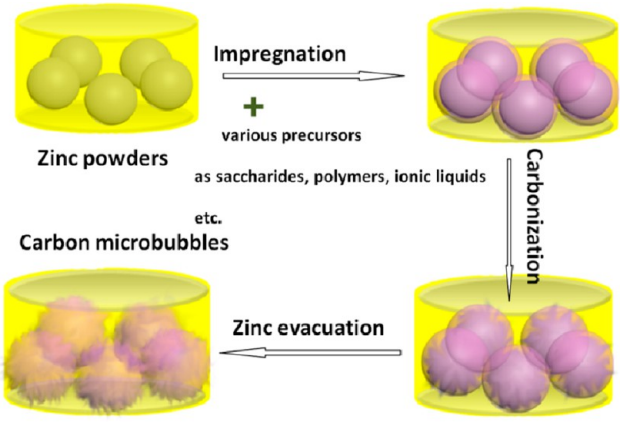

2. Physicochemical Characterization. Morphologies of the samples were characterized by thermal field emmission SEM (Quanta 400F) under 20 kV and TEM (FEI Tecnai G2 F30) under 300 kV. Structures, composition and elemental analysis were performed by XRD (D/MAX 2200 VPC), Raman (Nicolet NXR 9650), and XPS (ESCA Lab250). The surface area and pore analysis were carried out on a Micromeritics instrument(ASAP 2420) with N_2 as absorbate at 77 K. The specific surface area and pore distribution were evaluated on the basis of Brunauer–Emmett–Teller (BET) specific surface and Barrett–Joyner–Halenda (BJH) desorption pore.

3. Electrochemical Characterization. For electrochemical characterization, HPGCMBs and polyvinylidene fluoride with a weight ratio of 95:5 were mixed with a small amount of 1-methyl-2-pyrrolidinone (NMP) to form a slurry mixture. The HPGCMBs electrodes were fabricated by pasting the slurry mixture on copper foil by an automatic thick film coater (AFA-I). Then the coating film was desiccated in an vacuum chamber at 120 °C for 12 h. After that the foil is pressed by an electromotive roller (MR-100A) and tailored to appropriate size by a coin-type cell microtome (T-06) (S = 1.5 cm^2). The loadage of active materials (ca. 800 μg) on each piece was determined by a microbalance (d = 0.1 μg). Standard cells (CR2032) with the above tailored foils as working electrode and lithium foils as the reference and counter electrode, polypropylene micromembrane (Clegard 2500) as the separator, 1 M $LiPF_6$ in ethylene carbonate (EC) and diethyl carbonate (DEC) with a weight ratio of 1:1 as the electrolyte, were assembled in an Ar-filled universal glovebox with the Oxygen and water vapor pressure less than 0.3 ppm. The cyclic voltammogram scanning at 0.2 mVs^{-1} in voltage cutoff of 0–3 V and electrochemical impedance spectra scanning from 1 MHz to 0.01 Hz with an ac signal amplitude of 10 mV were performed on an Ivium electrochemical workstation. All the cells for cyclic voltammogram and electrochemical impedance tests are newly fabricated with an open circuit voltage ca. 3 V. For cycling and rate performance, the cells were galvanostatically charged and discharged in a volatage cutoff of 0.005–3 V at various rates on a mulitichannel Neware battery testing system.

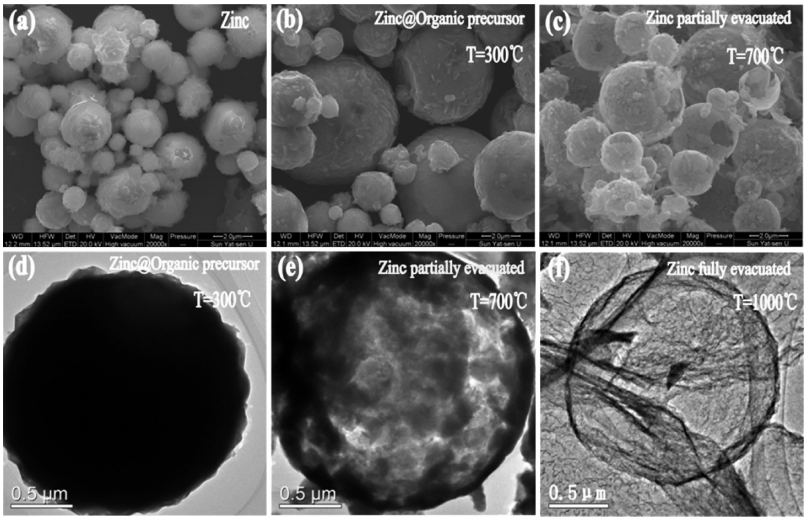

Figure 1. Evolution of HPGCMBs: SEM images for (a) zinc powder template, (b) the organic precursor impregnated Zinc powder carbonized at 300 °C for 1 h, and (c) the zinc powder@carbonized precursor annealed at 700 °C for 1 h, and TEM images for (d) the organic precursor impregnated zinc powder carbonized at 300 °C for 1 h, (e) the zinc powder@carbonized precursor annealed at 700 °C for 1 h, and (f) the zinc powder@carbonized precursor annealed at 1000 °C for 1 h.

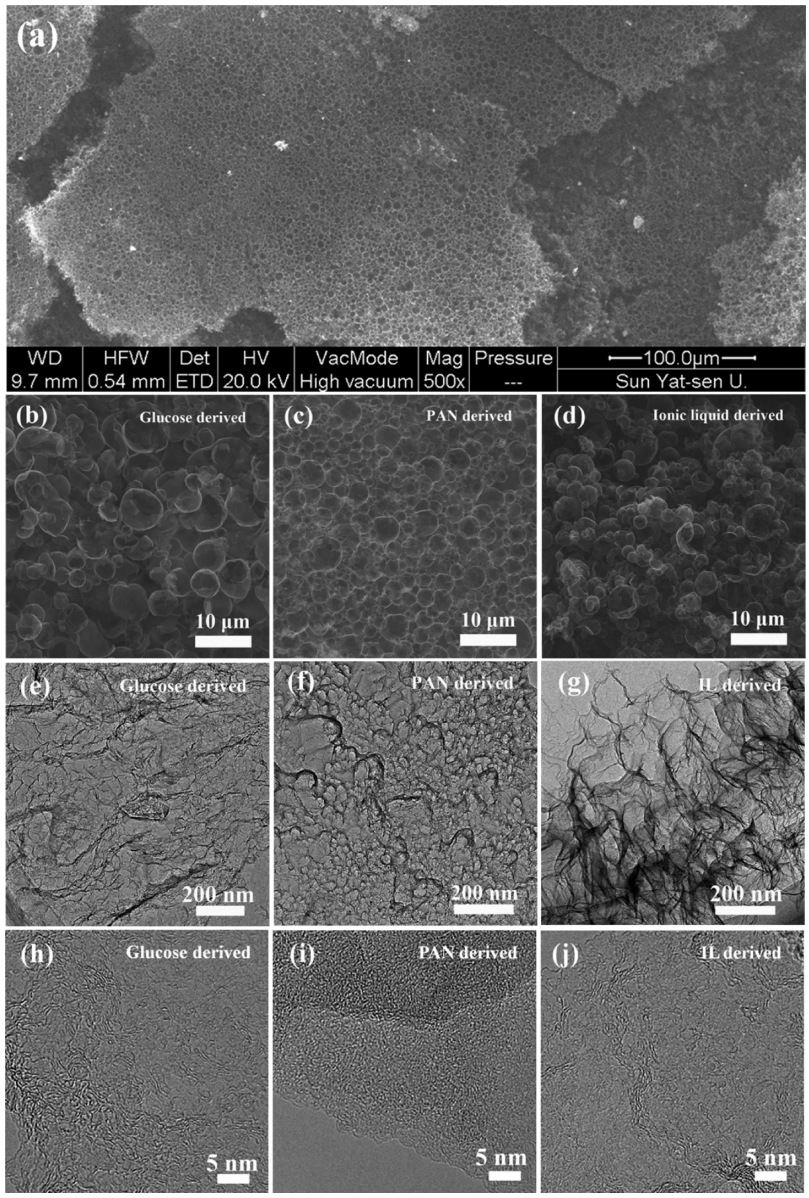

Figure 2. Morphologies and microstructures: (a) low-magnification SEM image for HPGCMBs; high-magnification SEM images for HPGCMBs derived from (b) glucose, (c) PAN, and (d) IL, TEM images for HPGCMBs derived from (e) glucose, (f) PAN, and (g) IL; and HRTEM images for HPGCMBs derived from (h) glucose (i) PAN, and (j) IL.

RESULTS AND DISCUSSION

Previously, we have reported carbon bubbles hybrid electrode achieved by zinc powder templated physical vapor deposition methods.[36,37] Those electrodes exhibited excellent electrochemical properties endowed by porous carbon bubble host and small active materials nanocrystals guest. Herein, we further this processes with series of organic precursor as substitutes for the costly carbon source (C_{60}). First, zinc powder is impregnated with heteroatom containing organic precursors which range from common imidazole-, pyridine-, pyrrole-, or piperidine-based ionic liquids or their derivatives, glucose and other saccharides, to polymers (e.g., PAN); then the impregnated zinc powder is heated to carbonize the precursors; last, the various heteroatom-doped HPGCMBs could be achieved through evacuation of zinc powder at high temperature. Figure 1a–f depicts the evolution of HPGCMBs in the whole process. SEM images (Figure 1a, b) show the Zinc@Organic precursor well-preserves the discrete spherical morphology of zinc template without agglomeration. This implies a very thin impregnation layer coating on the template which is well consistent with that presented in the TEM image (Figure 1d). With the elevation of annealing temperature, zinc@organic precursor suffers from carbonization of organic precursor and the evacuation of zinc template. Figure 1c, e shows the partial evacuation of zinc template brought about

Table 1. Element Content for the HPGCMBs Derived from Different Organic Precursors

XPS survey for HPGCMBs				
precursor	C content (at. %)	O content (at. %)	N content (at. %)	B content (at. %)
glucose	84.33	15.67	0	0
PAN	86.73	9.22	4.05	0
IL	73.83	16.38	7.99	1.08

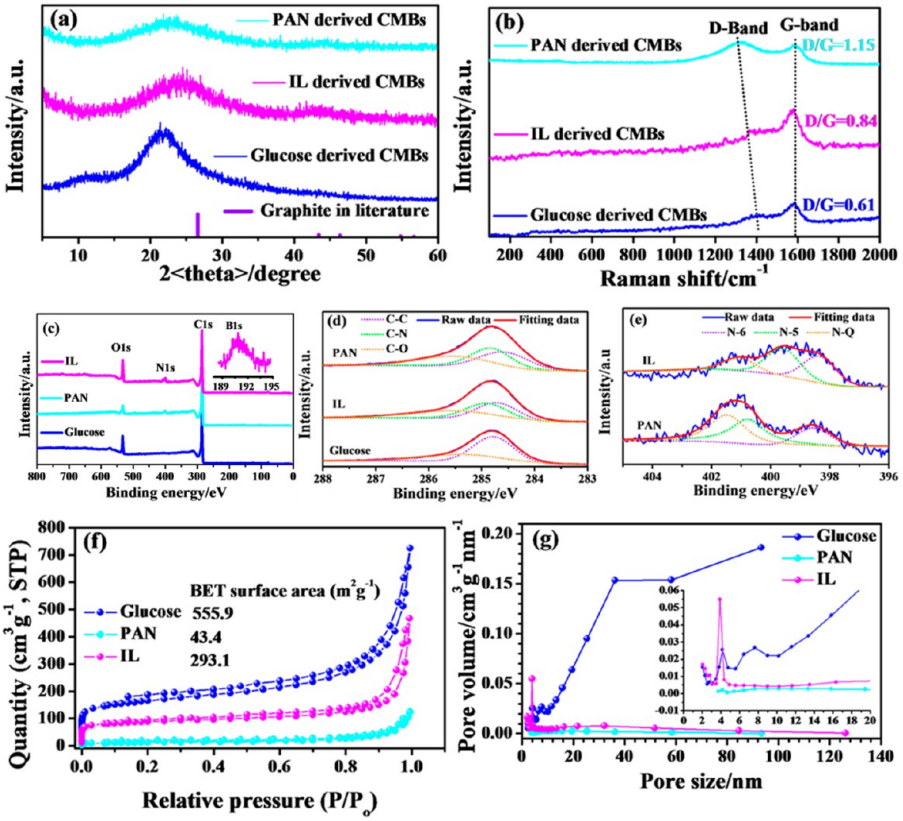

Figure 3. Structure, composition, surface area and pore analysis: (a) XRD patterns (b) Raman spectra, (c) XPS survey spectra, (d) C 1s and (e) N 1s local XPS spectra, (f) adsorption−desorption isotherms, and (g) BJH desorption pores distribution for HPGCMBs derived from different organic precursors.

porous microstructures in the carbon shell. After full evacuation, the carbon bubbles well retain the spherical skeleton of the template (Figure 1f).

Figure 2a presents the low-magnification SEM image of the HPGCMBs exhibiting honeycomb-like pads of several hundred micrometers assembled by porous carbon microbubbles. This indicates the availability of the approach in obtaining large amount of samples for scale application in energy storage and conversion. Figure 2b−d show HPGCMBs derived from different organic precursors. The common characteristic of porous openings and discrete spherical shells in the HPGCMBs implies the universality of the methodology. In the TEM images (Figure 2e−g), diverse creases verify the feasibility in altering the microstructures of HPGCMBs through changing different precursors. Moreover, the tunable aspects in microstructures also work for hierarchical pores, graphitic content, and doping species and amount as displayed in the HRTEM images and XPS analysis (Figure 2h−j and Table 1).

The XRD patterns in Figure 3a show all the HPGCMBs are similar to graphitic hard carbon with a diffuse X-ray peak near 22° (2θ) corresponding to ordered lattice spacing of 0.4 nm. The shift of this diffuse peak to higher diffraction angle implies shrinking of lattice spacing. This ordered lattice spacing and its shrinkage would influence the loading availability of guest ions. The peak about 43° (2θ) corresponds to diffraction of (110) surface in graphite (PDF No. 26−1079). The increasing of this peak indicates enhancing degree of graphitization, while that near 10° (2θ) assert exfoliated graphite layers by oxygen functional groups or oxidation of graphite.[38] Hence, the characteristic peaks in XRD patterns imply the disparity of the extents of graphitization and oxidation in the HPGCMBs. Moreover, the graphitization also could be evaluated by the ratio of D band to G band in Raman spectra (Figure 3b). The former band relates to turbostratic structure in sp2 hybrid graphite layer or sp3 hybridized carbon, whereas the latter one derives from sp^2 hybrid graphite carbon.[39] Therefore, a higher I_D/I_G implies a lower graphitic content. As depicted in Raman spectra, the graphitization is readily altered by changing the precursor species.

Except for varying graphitic content, an adjustable heteroatoms doping is also easily realized. In the XPS survey spectra (Figure 3c), the glucose derived HPGCMBs mainly consist of C, and O with a doping ratio of 15.67% in atomic content, whereas PAN-derived HPGCMBs realize the codoping of N and O with 13.27% doping ratio. Remarkably, the doping ratio could be elevated to 26.17% through utilizing an ionic liquid containing N, O, and B (Table 1). On the basis of the analysis of the local XPS spectra (Figure 3d), the deconvoluted C 1s spectrum implies the coexistence of C−C, C−O and/or C−N bonding in different HPGCMBs.[18] For the N-doped HPGCMBs (Figure 3e), the N 1s spectrum can be deconvoluted into three peaks ascribed to pyridinc N (N-6), pyrrolic N (N-5), and graphitic N (N-Q), respectively.[16,26,32,40] They both verify different heteroatoms doped HPGCMBs could be readily obtained through varying the organic precursors containing the specific atoms. These doping atoms would not only bring about abundant radical functional groups availing for ions adsorption, but also probably influence the formation of specific microstructures and hierarchical pores.[18,33,34,41]

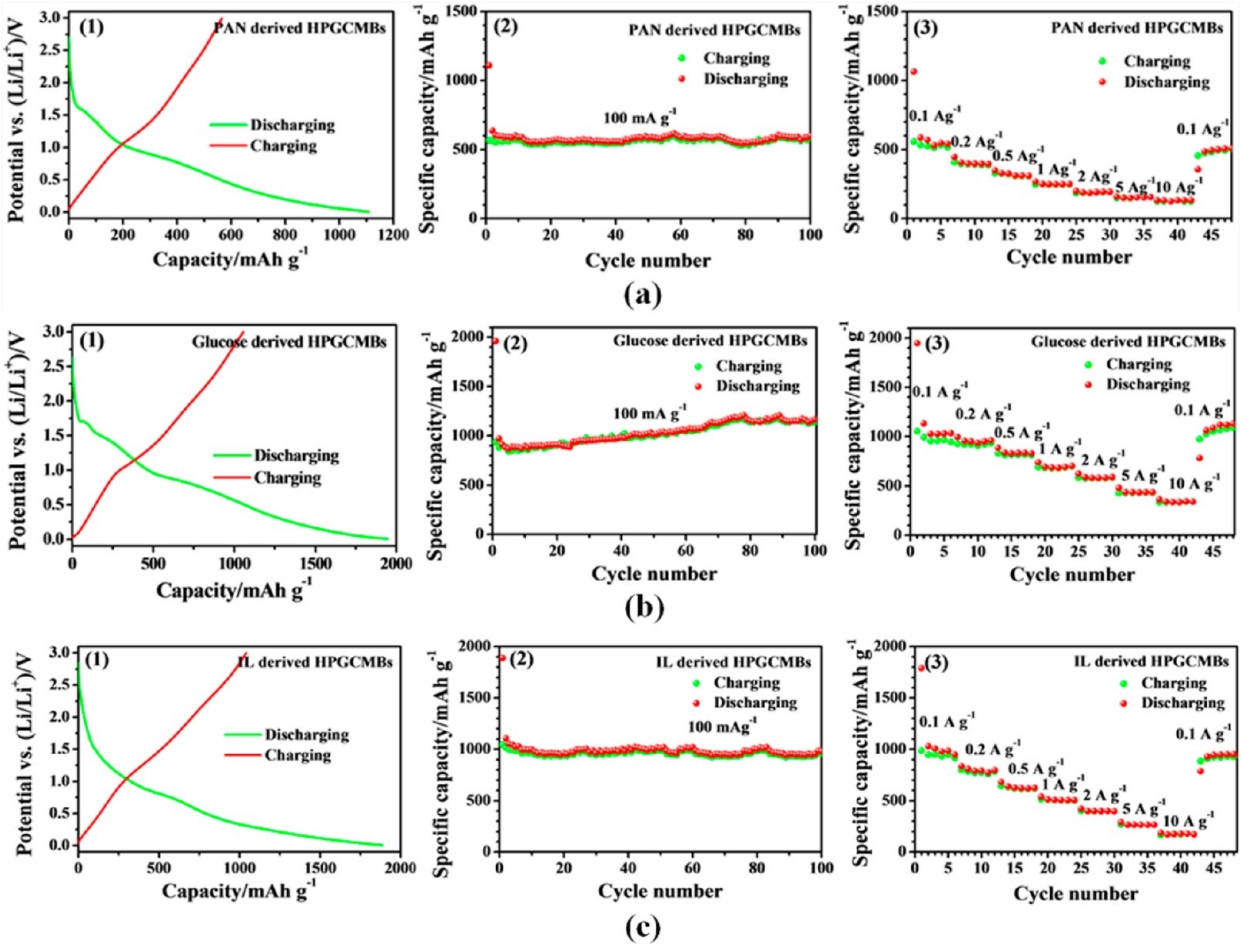

Figure 4. Electrochemical performance for (a) PAN-derived HPGCMBs electrodes (1) typical charge−discharge curve tested at 0.1 A g^{-1}, (2) cycle performance tested at 0.1 A g^{-1}, and (3) rate performance tested at varying current from 0.1 A g^{-1} to 10 A g^{-1}, (b) glucose derived HPGCMBs electrodes (1) typical charge−discharge curve tested at 0.1 A g^{-1}, (2) cycle performance tested at 0.1 A g^{-1}, and (3) rate performance tested at varying current from 0.1 A g^{-1} to 10 A g^{-1}, and (c) IL derived HPGCMBs electrodes (1) typical charge−discharge curve tested at 0.1 A g^{-1}, (2) cycle performance tested at 0.1 A g^{-1}, and (3) rate performance tested at varying current from 0.1 A g^{-1} to 10 A g^{-1}.

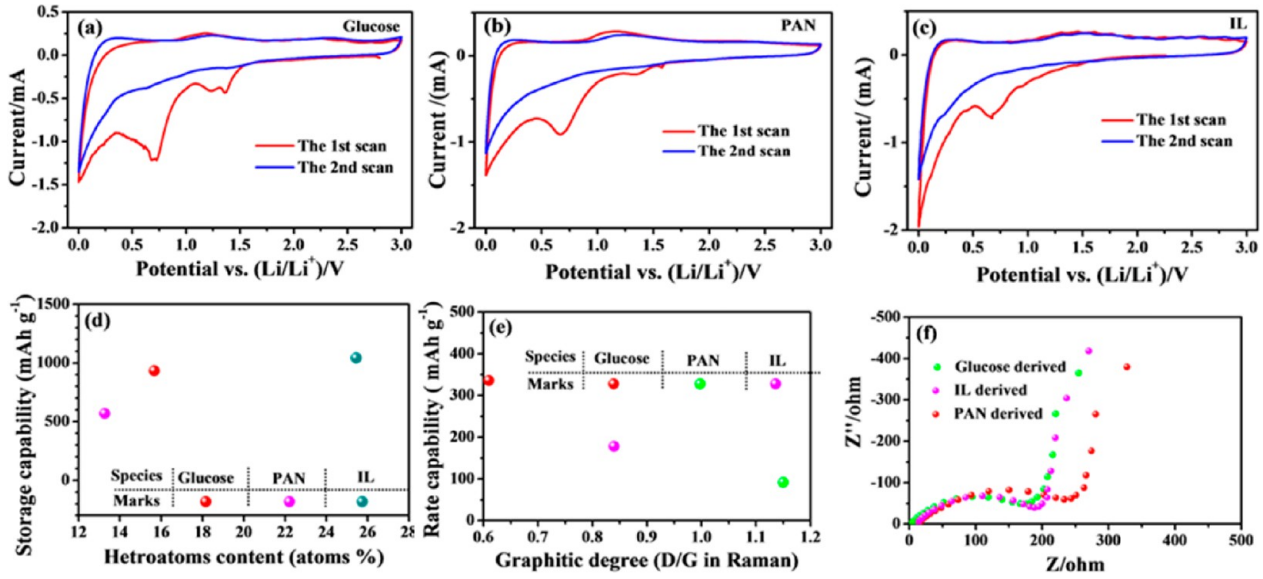

Figure 5. Electrochemical analysis: cyclic voltammograms for HPGCMBs electrodes derived from (a) glucose, (b) PAN, and (c) IL, (d) the relation of heteroatoms content to storage capability in HPGCMBs electrodes, (e) the relation of graphitic content to rate capability in HPGCMBs electrodes, and (f) the electrochemical impedance spectra for HPGCMBs electrodes.

dx.doi.org/10.1021/am506747z | ACS Appl. Mater. Interfaces 2014, 6, 21661−21668

Figure 3f presents the adsorption and desorption isotherms for the different HPGCMBs. They show similar type II isotherms.[42,43] On the basis of the isotherms, BET surface areas of 43.4, 293.1, and 555.9 $m^2 g^{-1}$ are attained for PAN, IL, and Glucose derived HPGCMBs, respectively. BJH pore distribution (Figure 3g) depict the IL derived HPGCMBs mainly contain mesopores ca. 4 nm with accumulated pore volume of 0.64 $cm^3 g^{-1}$ (pore diameter from 1.7 to 300 nm), whereas hierarchal pore distribution is realized for PAN and glucose derived HPGCMBs with pore volumes reaching 0.18 and 1.01 $cm^3 g^{-1}$, respectively. Summarily, this universal methodology could realize adjustable graphic content, heteroatoms doping species and amount in HPGCMBs in the meantime.

To exemplify the virtues of the HPGCMBs in practice, state-of-the-art anodes for lithium-ion batteries are tested. Figure 4 presents the electrochemical performance of the HPGCMBs derived from different organic precursors. For the PAN-derived HPGCMB electrode (Figure 4a), an initial capacity of 1100 mAh g^{-1} is achieved. Reversible capacity about 600 mAh g^{-1} could be attained steadily maintaining for 100 cycles equivalent to initial Coulombic efficiency 55%. When altering rates, it obtains capacity of 594 mAh g^{-1} at 0.1 A g^{-1}, 435 mAh g^{-1} at 0.2 A g^{1-}, 344 mAh g^{-1} at 0.5 A g^{-1}, 253 mAh g^{-1} at 1 A g^{-1}, and 128 mAh g^{-1} at 10 A g^{-1} respectively. As to the HPGCMBs derived from glucose and IL (Figure 4b, c), stable cycling performance is readily maintained with much higher capacity of 1056 mAh g^{-1} and 1041 mAh g^{-1}, respectively. Besides, enhancing rate performance of 1041 mAh g^{-1} at 0.1 A g^{-1}, 830 mAh g^{-1} at 0.2 A g^{-1}, 678 mAh g^{-1} at 0.5 A g^{-1}, 534 mAh g^{-1} at 1 A g^{-1}, and 178 mAh g^{-1} at 10 A g^{-1} is obtained for the IL-derived HPGCMB electrode. Importantly, at large rate of 10 A g^{-1}, the glucose-derived HPGCMB electrode exhibits a high capacity of 370 mAh g^{-1}. Comparing to HPGCMBs derived from PAN, the improvement of cycling and rate performance for glucose and IL derived HPGCMBs maybe relate to not only the modifying of microstructures but also the enlarged specific surface area and hierarchical pores. Moreover, the marked graphitization, doping species, and amount are also relevant to the superior lithium-ion storage capability and rate capability.

As exhibited in the typical cyclic voltammograms (Figure 5a–c), the first cathode scans are characteristic of three series of peaks centered at about 1.4 and 1.2, 0.7, and 0 V, whereas the anode scans exhibit peaks centered at 0.2, 1.2, and 2.4 V. In the cathode scans, the former two peaks maybe involve the reduction of oxygen or nitrogen functional groups in the HPGCMBs.[44,45] The peak about 0.7 V is generally attributed to the formation of Li_2O and some Li containing solid electrolyte interphase (SEI), and the peak ca. 0 V ascribed to intercalation of Li^+ into sp2 hybrid graphitic carbon like graphite and graphene based carbon composites.[16,41,46–49] In comparison with the second scans, the weakening for the former three peaks indicates the reduction of doping atoms related functional groups and the formation of SEI are largely irreversible. According to the anode scans, the deintercalation of Lithium ions from graphitic carbon near 0.2 V and delithiation Li_2O near 1.2 V in doping HPGCMBs are highly reversible.[23,48,50] The slight peak about 2.4 V is related to reoxidation of those already reduced oxygen or nitrogen functional groups.[44,45] To further clarify the microstructure- and doping-related influence on the electrochemical properties of the HPGCMBs electrodes, we present the relations of graphitic content and doping amount to lithium-ion storage capability and rate capability in Figure 5d, e. Evidently, increasing the doping amount is suitable for achieving much superior ion storage capability and severe graphitization (a lower ratio of D/G) favors of improving the rate capability. By changing the precursors, the doping amount and graphitization are readily optimized for obtaining advanced electrodes with superior storage capability and good rate performance. The improved rate performance implies easier charge transfer, which is consistent with the decrease in charge transfer resistance for about 20% from PAN-derived HPGCMBs to those derived from IL and glucose depicted in the electrochemical impedance spectra (Figure 5f).

CONCLUSION

In summary, we develop a facile strategy to fabricate HPGCMBs; this general methodology affords to generate abundant microstructures, adjustable graphitic content and doping species and amount in the carbon nanostructures. Benefiting from those hierarchical porous structures, abundant doping atoms, and appropriate graphitization, fast kinetic processes and superior ion transfer and storage are perfectly combined. Besides large ion storage capability, those HPGCMB electrodes also exhibit superior cyclibility and rate performance. Actually, those unique structures are applicable to other fields as catalyst support, host–guest chemistry other than lithium-ion batteries.

AUTHOR INFORMATION

Corresponding Author

*E-mail: wchengx@mail.sysu.edu.cn. Tel. & Fax: +86-20-84113901.

Notes

The authors declare no competing financial interest.

ACKNOWLEDGMENTS

This work was financially supported by the National Natural Science Foundation of China (51125008 and 11274392) and the Doctoral Innovative Talents Cultivation Project in Sun Yat-sen (Zhongshan) University.

REFERENCES

(1) Arico, A. S.; Bruce, P.; Scrosati, B.; Tarascon, J. M.; van Schalkwijk, W. Nanostructured Materials for Advanced Energy Conversion and Storage Devices. *Nat. Mater.* **2005**, *4*, 366–377.

(2) Armand, M.; Tarascon, J. M. Building Better Batteries. *Nature* **2008**, *451*, 652–657.

(3) Xu, S.; Zhang, Y.; Cho, J.; Lee, J.; Huang, X.; Jia, L.; Fan, J. A.; Su, Y.; Su, J.; Zhang, H.; Cheng, H.; Lu, B.; Yu, C.; Chuang, C.; Kim, T.; Song, T.; Shigeta, K.; Kang, S.; Dagdeviren, C.; Petrov, I.; Braun, P. V.; Huang, Y.; Paik, U.; Rogers, J. A. Stretchable Batteries with Self-similar Serpentine Interconnects and Integrated Wireless Recharging Systems. *Nat. Commun.* **2013**, *4*, 1543.

(4) Whittingham, M. S. Lithium Batteries and Cathode Materials. *Chem. Rev.* **2004**, *104*, 4271–301.

(5) Slater, M. D.; Kim, D.; Lee, E.; Johnson, C. S. Sodium-Ion Batteries. *Adv. Funct. Mater.* **2013**, *23*, 947–958.

(6) Pang, C.; Cui, H.; Yang, G.; Wang, C. Flexible Transparent and Free-Standing Silicon Nanowires Paper. *Nano Lett.* **2013**, *13*, 4708–4714.

(7) Jin, S.; Li, N.; Cui, H.; Wang, C. Growth of the Vertically Aligned Graphene@ Amorphous GeOx Sandwich Nanoflakes and Excellent Li Storage Properties. *Nano Energy* **2013**, *2*, 1128–1136.

(8) Li, N.; Song, H.; Cui, H.; Wang, C. Sn@Graphene Grown on Vertically Aligned Graphene for High-capacity, High-rate, and Long-life Lithium Storage. *Nano Energy* **2014**, *3*, 102−112.
(9) Fan, J.; Wang, T.; Yu, C.; Tu, B.; Jiang, Z.; Zhao, D. Ordered, Nanostructured Tin-Based Oxides/Carbon Composite as the Negative-Electrode Material for Lithium-Ion Batteries. *Adv. Mater.* **2004**, *16*, 1432−1436.
(10) Zou, Y.; Wang, Y. Sn@CNT Nanostructures Rooted in Graphene with High and Fast Li-Storage Capacities. *ACS Nano* **2011**, *5*, 8108−8114.
(11) Wang, Y.; Li, B.; Zhang, C.; Tao, H.; Kang, S.; Jiang, S.; Li, X. Simple Synthesis of Metallic Sn Nanocrystals Embedded in Graphitic Ordered Mesoporous Carbon Walls as Superior Anode Materials for Lithium Ion Batteries. *J. Power Sources* **2012**, *219*, 89−93.
(12) Li, X.; Wang, C. Engineering Nanostructured Anodes via Electrostatic Spray Deposition for High Performance Lithium Ion Battery Application. *J. Mater. Chem. A* **2013**, *1*, 165−182.
(13) Zhou, H.; Zhu, S.; Hibino, M.; Honma, I.; Ichihara, M. Lithium Storage in Ordered Mesoporous Carbon (CMK-3) with High Reversible Specific Energy Capacity and Good Cycling Performance. *Adv. Mater.* **2003**, *15*, 2107−2111.
(14) Wang, D. W.; Li, F.; Liu, M.; Lu, G. Q.; Cheng, H. M. 3D Aperiodic Hierarchical Porous Graphitic Carbon Material for High-Rate Electrochemical Capacitive Energy Storage. *Angew. Chem., Inter. Ed.* **2008**, *47*, 373−376.
(15) Zhang, L. L.; Zhao, X.; Stoller, M. D.; Zhu, Y. W.; Ji, H. X.; Murali, S.; Wu, Y. P.; Perales, S.; Clevenger, B.; Ruoff, R. S. Highly Conductive and Porous Activated Reduced Graphene Oxide Films for High-Power Supercapacitors. *Nano Lett.* **2012**, *12*, 1806−1812.
(16) Qie, L.; Chen, W. M.; Wang, Z. H.; Shao, Q. G.; Li, X.; Yuan, L. X.; Hu, X. L.; Zhang, W. X.; Huang, Y. H. Nitrogen-Doped Porous Carbon Nanofiber Webs as Anodes for Lithium Ion Batteries with a Superhigh Capacity and Rate Capability. *Adv. Mater.* **2012**, *24*, 2047−2050.
(17) Mukhopadhyay, A.; Guo, F.; Tokranov, A.; Xiao, X. C.; Hurt, R. H.; Sheldon, B. W. Engineering of Graphene Layer Orientation to Attain High Rate Capability and Anisotropic Properties in Li-Ion Battery Electrodes. *Adv. Funct. Mater.* **2013**, *23*, 2397−2404.
(18) Song, H.; Li, N.; Cui, H.; Wang, C. Enhanced Storage Capability and Kinetic Processes by Pores- and Hetero-atoms- riched Carbon Nanobubbles for Lithium-ion and Sodium-ion Batteries Anodes. *Nano Energy* **2014**, *4*, 81−87.
(19) He, W.; Lu, L. Revisiting the Structure of Graphene Oxide for Preparing New-Style Graphene-Based Ultraviolet Absorbers. *Adv. Funct. Mater.* **2012**, *22*, 2542−2549.
(20) Paraknowitsch, J. P.; Zhang, J.; Su, D.; Thomas, A.; Antonietti, M. Ionic Liquids as Precursors for Nitrogen-Doped Graphitic Carbon. *Adv. Mater.* **2010**, *22*, 87−92.
(21) Ma, F. W.; Zhao, H.; Sun, L. P.; Li, Q.; Huo, L. H.; Xia, T.; Gao, S.; Pang, G. S.; Shi, Z.; Feng, S. H. A Facile Route for Nitrogen-doped Hollow Graphitic Carbon Spheres with Superior Performance in Supercapacitors. *J. Mater. Chem.* **2012**, *22*, 13464−13468.
(22) Li, X.; Geng, D.; Zhang, Y.; Meng, X.; Li, R.; Sun, X. Superior Cycle Stability of Nitrogen-doped Graphene Nanosheets as Anodes for Lithium Ion Batteries. *Electrochem. Commun.* **2011**, *13*, 822−825.
(23) Li, X.; Liu, J.; Zhang, Y.; Li, Y.; Liu, H.; Meng, X.; Yang, J.; Geng, D.; Wang, D.; Li, R.; Sun, X. High Concentration Nitrogen Doped Carbon Nanotube Anodes with Superior Li+ Storage Performance for Lithium Rechargeable Battery Application. *J. Power Sources* **2012**, *197*, 238−245.
(24) Srinivas, K.; Vithal, M.; Sreedhar, B.; Raja, M. M.; Reddy, P. V. Structural, Optical, and Magnetic Properties of Nanocrystalline Co Doped SnO_2 Based Diluted Magnetic Semiconductors. *J. Phys. Chem. C* **2009**, *113*, 3543−3552.
(25) Srivastava, J. K.; Pandey, Preeti; Mishra, V. N.; Dwivedi, R. Sensing Mechanism of Pd-doped SnO_2 Sensor for LPG Detection. *Solid State Sci.* **2009**, *11*, 1602−1605.
(26) Chen, S.; Bi, J.; Zhao, Y.; Yang, L.; Zhang, C.; Ma, Y.; Wu, Q.; Wang, X.; Hu, Z. Nitrogen-Doped Carbon Nanocages as Efficient Metal-Free Electrocatalysts for Oxygen Reduction Reaction. *Adv. Mater.* **2012**, *24*, 5593−5597.
(27) Huang, H. T.; Tian, S. Q.; Xu, J.; Xie, Z.; Zeng, D. W.; Chen, D.; Shen, G. Z. Needle-like Zn-doped SnO_2 Nanorods with Enhanced Photocatalytic and Gas Sensing Properties. *Nanotechnology* **2012**, *23*, 105502.
(28) Yang, G.; Song, H.; Cui, H.; Wang, C. $(\alpha\text{-}Fe_2O_3)_{1\text{-}x}(V_2O_5)_x$ Solid Solutions: An Excellent Lithium Ion Anodes Material. *Nano Energy* **2014**, *5*, 9−19.
(29) Zhao, Y.; Yang, L.; Chen, S.; Wang, X.; Ma, Y.; Wu, Q.; Jiang, Y.; Qian, W.; Hu, Z. Can Boron and Nitrogen Co-doping Improve Oxygen Reduction Reaction Activity of Carbon Nanotubes? *J. Am. Chem. Soc.* **2013**, *135*, 1201−1204.
(30) Neamen, D. A. *Semiconductor Physics and Devices Basic Principles*, 4th ed.; McGraw−Hill Higher Education: New York, 2012.
(31) Wu, Z. S.; Xue, L.; Ren, W.; Li, F.; Wen, L.; Cheng, H. M. A LiF Nanoparticle-Modified Graphene Electrode for High-Power and High-Energy Lithium Ion Batteries. *Adv. Funct. Mater.* **2012**, *22*, 3290−3297.
(32) Chen, L. F.; Zhang, X. D.; Liang, H. W.; Kong, M.; Guan, Q. F.; Chen, P.; Wu, Z. Y.; Yu, S. H. Synthesis of Nitrogen-doped Porous Carbon Nanofibers as an Efficient Electrode Material for Supercapacitors. *ACS Nano* **2012**, *6*, 7092−7102.
(33) Das, D.; Kim, S.; Lee, K. R.; Singh, A. K. Li Diffusion through Doped and Defected Graphene. *Phys. Chem. Chem. Phys.* **2013**, *15*, 15128−15134.
(34) Paraknowitsch, J. P.; Thomas, A. Doping Carbons beyond Nitrogen: an Overview of Advanced Heteroatom Doped Carbons with Boron, Sulphur and Phosphorus for Energy Applications. *Energy Environ. Sci.* **2013**, *6*, 2839−2855.
(35) Yue, L.; Zhong, H.; Tang, D.; Zhang, L. Porous Si Coated with S-doped Carbon as Anode Material for Lithium Ion Batteries. *J. Solid State Electrochem.* **2013**, *17*, 961−968.
(36) Yang, G. Z.; Song, H. W.; Cui, H.; Liu, Y. C.; Wang, C. X. Ultrafast Li-ion Battery Anode with Superlong Life and Excellent Cycling Stability from Strongly Coupled ZnO Nanoparticle/Conductive Nanocarbon Skeleton Hybrid Materials. *Nano Energy* **2013**, *2*, 579−585.
(37) Song, H.; Yang, G.; Cui, H.; Wang, C. Electrodes Engineering of High power, Long life and Excellent Cycling Stability for Rechargeable Lithium Batteries. *Nano Energy* **2014**, *3*, 16−25.
(38) Marcano, D. C.; Kosynkin, D. V.; Berlin, J. M.; Sinitskii, A.; Sun, Z.; Slesarev, A.; Alemany, L. B.; Lu, W.; Tour, J. M. Improved Synthesis of Graphene Oxide. *ACS Nano* **2010**, *4*, 4806−4814.
(39) Dillon, R. O.; Woollam, J. A.; Katkanant, V. Use of Raman Scattering to Investigate Disorder and Crystallite Formation in As-deposited and Annealed Carbon Films. *Phys. Rev. B* **1984**, *29*, 3482−3489.
(40) Liu, S.; Tian, J.; Wang, L.; Zhang, Y.; Qin, X.; Luo, Y.; Asiri, A. M.; Al-Youbi, A. O.; Sun, X. Hydrothermal Treatment of Grass: A Low-Cost, Green Route to Nitrogen-Doped, Carbon-Rich, Photoluminescent Polymer Nanodots as an Effective Fluorescent Sensing Platform for Label-Free Detection of Cu(II) Ions. *Adv. Mater.* **2012**, *24*, 2037−2041.
(41) Fan, X.; Zheng, W. T.; Kuo, J. L. Adsorption and Diffusion of Li on Pristine and Defective Graphene. *ACS Appl. Mater. Interfaces* **2012**, *4*, 2432−8.
(42) Brunauer, S.; Emmett, P. H.; Teller, E. Adsorption of Gases in Multimolecular Layers. *J. Am. Chem. Soc.* **1938**, *60*, 309−319.
(43) Hubbard, A. T. *Encyclopedia of Surface and Colloid Science*; Marcel Dekker: New York, 2002.
(44) Byon, H. R.; Gallant, B. M.; Lee, S. W.; Shao-Horn, Y. Role of Oxygen Functional Groups in Carbon Nanotube/Graphene Free-standing Electrodes for High Performance Lithium Batteries. *Adv. Funct. Mater.* **2013**, *23*, 1037−1045.
(45) Mao, Y.; Duan, H.; Xu, B.; Zhang, L.; Hu, Y.; Zhao, C.; Wang, Z.; Chen, L.; Yang, Y. Lithium storage in nitrogen-rich mesoporous carbon materials. *Energy Environ. Sci.* **2012**, *5*, 7950−7955.

(46) Fong, R.; von Sacken, U.; Dahn, J. R. Studies of Lithium Intercalation into Carbons Using Nonaqueous Electrochemical Cells. *J. Electrochem. Soc.* **1990**, *137*, 2009−2013.
(47) Shu, Z. X.; McMillan, R. S.; Murray, J. J. Electrochemical Intercalation of Lithium into Graphite. *J. Electrochem. Soc.* **1993**, *140*, 922−927.
(48) Sato, K.; Noguchi, M.; Demachi, A.; Oki, N.; Endo, M. A Mechanism of Lithium Storage in Disordered Carbons. *Science* **1994**, *264*, 556−558.
(49) Lee, S. H.; Sridhar, V.; Jung, J. H.; Karthikeyan, K.; Lee, Y. S.; Mukherjee, R.; Koratkar, N.; Oh, I. K. Graphene-Nanotube-Iron Hierarchical Nanostructure as Llithium Ion Battery Anode. *ACS Nano* **2013**, *7*, 4242−4251.
(50) Ren, W.; Li, D.; Liu, H.; Mi, R.; Zhang, Y.; Dong, L.; Dong, L. Lithium Storage Performance of Carbon Nanotubes with Different Nitrogen Contents as Anodes in Lithium Ions Batteries. *Electrochim. Acta* **2013**, *105*, 75−82.